Very high cycle fatigue (VHCF) behavior of structured Al 2024 thin sheets

Sebastian Stille*, Tilmann Beck, Lorenz Singheiser

Institute of Energy and Climate Research (IEK-2), FZ Juelich, D-52425 Juelich, Germany
* Corresponding author: s.stille@fz-juelich.de

Abstract In the present study the VHCF behavior of Al 2024, a standard material in aerospace application, is investigated. The focus of the presented work is the influence of riblet-like surface structures on fatigue life and damage mechanisms. The cold-rolling process used for riblet forming results in slight work hardening and near-surface residual stresses. Furthermore the influence of pure Al-claddings on the VHCF behavior of Al 2024 sheets is examined. Fatigue tests are performed using an ultrasonic fatigue testing system at a frequency of around 20 kHz. The present work contributes to a deeper understanding of riblet structures and surface claddings on the VHCF behavior of Al 2024.

Keywords VHCF, Al 2024, surface structure

1. Introduction

An innovative approach for aerodynamic drag reduction, e.g. of airfoils, are surface riblet structures [1] combined with transversal surface waves with amplitudes of few 1/10 mm at frequencies of some 100 Hz [2]. The resulting very high cycle fatigue (VHCF) loading at cycle numbers beyond the value of $2x10^7$, taken as ultimate cycle number in most studies on fatigue of Al sheet alloys for aircraft application, has to be considered as a limiting factor for this approach.

Al 2024 is a standard material in aerospace applications. Its VHCF behavior has been evaluated in detail in different studies [3-7]. These contributions show that material failure takes place even beyond $2x10^7$ load cycles and that the S/N curve does not approach a horizontal fatigue limit. Fatigue experiments on cladded sheets have been performed in references [8-10]. Merati et al. [8] observed multiple crack initiation sites at the cladding layer in the regime up to $6x10^5$ cycles. Edwards et al. [9] report that the first crack in the cladding layer can be detected as early as 1 % of the total lifetime of the samples and that clad specimen are less sensitive to notching effects than bare Al 2024 sheets.

One intention of the present work is the investigation of the VHCF behavior of clad Al 2024 material up to cycle numbers distinctly beyond the existing data. Furthermore, the influence of riblet structures on the VHCF life of Al 2024 sheets needs to be determined for future application of active drag reduction. The experiments conducted in the frame of the present study cover nano-indentation, X-ray stress analysis, ultrasonic fatigue experiments and electron microscopy based fractography.

2. Material

The experiments were performed on the aluminium alloy Al 2024. The sheet material has been supplied by ALCOA Mill Products in the T-351 state (solutions heat treated at 493 °C and quenched in water, subsequently stress relieved by stretching to a controlled deformation and finally naturally aged for 8 days [11]). The sheets are supplied in two different thicknesses, 1.6 and 2 mm. Furthermore, sheets with a cladding layer of 64 µm of pure aluminium on one side were tested.

Table 1: Chemical composition of the investigated Al2024 material

Material	Cu	Fe	Mg	Mn	Si	Ti	Zn
Weight-%	4.58	0.21	1.48	0.47	0.073	0.016	0.098

Table 2: Key mechanical properties of Al2024 in the T-351 state

Young's modulus, E [12]	Yield strength, $R_{p0.2}$	Ultimate tensile strength	Elongation at break
73.1 GPa	321.5 MPa	446.5 MPa	18.5 %

Prior to testing the chemical composition of the material was analyzed by inductively coupled plasma optical emission spectroscopy (ICP-OES). The results are listed in Table 1. The key mechanical properties are listed in Table 2 (values determined by the supplier).

An important aspect of the present work is the influence of the surface state of the material on its VHCF behavior. As shown e.g. in reference [13], scratches significantly reduce the lifetime of clad Al 2024 sheets. To overcome this problem, fatigue samples are usually grinded and polished. This standard process to assure reproducible smooth surfaces is not applicable for clad material, since surface grinding and polishing would remove the thin cladding layer. A detailed analysis of the as-received specimen surface has thus been performed. Scratches on clad samples can be described as small notches with a diameter of a few µm in arbitrary orientation.

3. Experimental setup

For fatigue testing an ultrasonic fatigue testing machine, developed at BOKU Vienna, is employed. The testing system is described in references [14] and [15]. Modifications made on the system are described in detail in reference [16]. The sample geometry is presented in Fig. 1(b). Sheet samples are laser cut to their final geometry. The volume (surface) of the gage length is 64 mm^3 (105.6 mm^2) for 1.6 mm thick sheets and 80 mm^3 (112 mm^2) for 2 mm thick sheets, respectively.

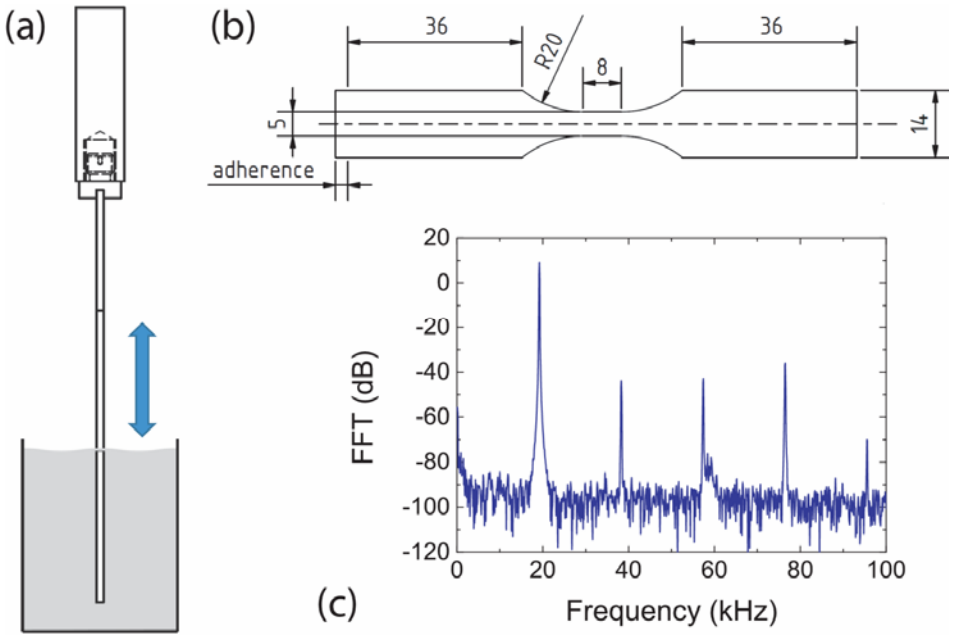

Figure 1. (a) Flat specimen connected to the load frame by an adapter and submerged in its lower part in glycerin. **(b)** Sample geometry. **(c)** Typical FFT spectrum of the vibration signal

The flat sheet samples are glued to an adapter which is connected via a thread to the testing machine. To avoid flexural vibrations, which have been observed in first experiments, samples are damped by submerging their lower part in glycerin during cyclic loading (cf. Fig 1(a)). In-situ monitoring of the sample vibration (Fig. 1(c)) shows a clean harmonic spectrum which is free of bending oscillations. All fatigue tests were performed at a frequency of around 20 kHz at room temperature and zero mean stress.

For further analysis, polished cross sections were prepared by embedding the samples in epoxy resin. The surface has been grinded with sand paper up to grade 1000 and subsequently polished with diamond paste. Indentation measurements were performed using a Berkovic type indenter. Fracture planes were analyzed in detail by scanning electron microscopy (SEM).

4. Results

4.1 Effects of riblet rolling

The cold working of the sheets during riblet forming lets expect the occurrence of work hardening as well as a surface-near stress. Therefore micro-indentation tests were performed on cross sections of flat as well as on riblet structured material. An indentation load of 5 mN was used.

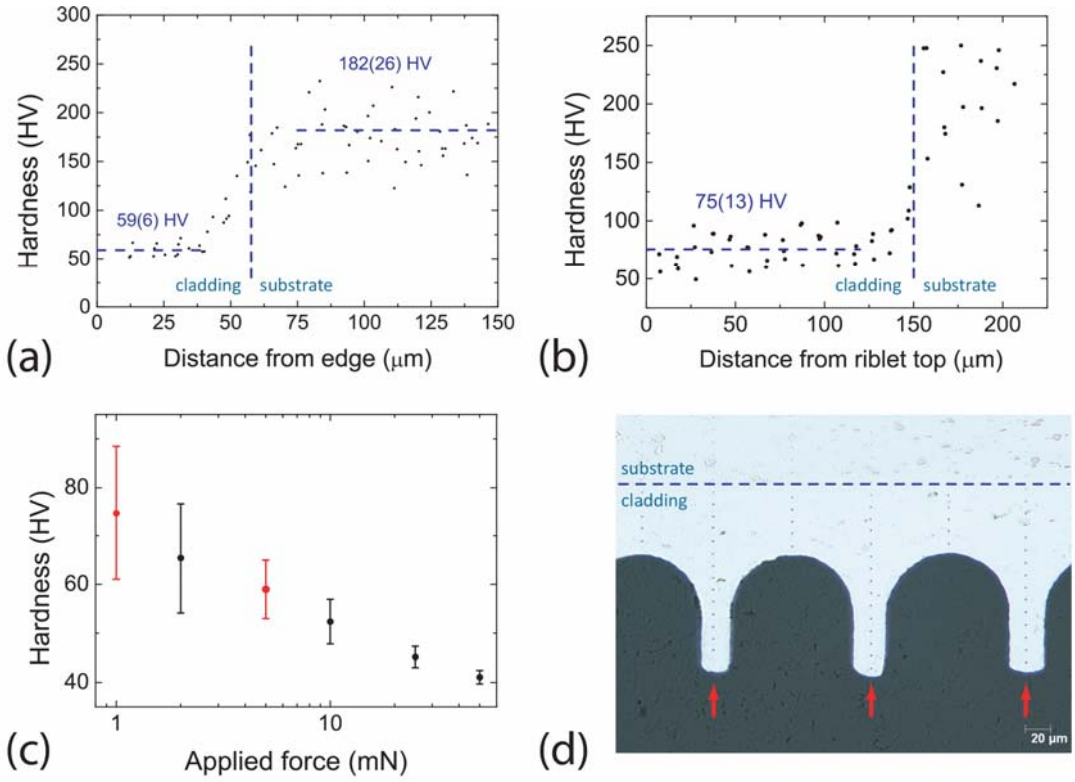

Figure 2. Microhardness measurements at clad material with and without riblet structure: **(a)** As-received (non-structured) material, $F = 5$ mN. The hardness is plotted against the distance from the cladding surface. **(b)** Structured material, $F = 1$ mN. The hardness is plotted against the distance from the riblet top. **(c)** Hardness of the cladding layer against the indentation load. **(d)** Polished cross-section of a structured sample. The measurements in Fig. 2(b) were performed in direction of the red arrows.

The results are presented in Fig. 2. Measurements on cladded sheets (Fig. 2(b)) show a hardness of (59 ± 6) HV0.005 for the cladding layer and of (182 ± 26) HV0.005 for the substrate. Measurements on structured samples were performed according to Fig. 2(d). The riblet structure is completely located in the cladding layer and does not affect the substrate. Since the riblets are quite narrow a smaller indentation load of 1 mN was applied to reduce the lateral size of the indentation. In spite of the strong local deformation during riblet forming, a nearly homogenous hardness of (75 ± 13) HV0.001 has been determined along the riblets and in the underlying part of the cladding. To investigate the influence of indentation load on the measured hardness, a series of indentation tests has been carried out in the cladding layer by performing 10 indentations at each of 6 forces in the range between 1 mN and 50 mN. The results are given in Fig. 2(c). A clear indentation-size effect is observed. Comparing the hardness values for 1 mN and 5 mN in Fig. 2(c) with cladding hardnesses in Figs. 2(a) and 2(b), it can concluded that the apparently increased hardness of the riblet structure can be completely attributed to the indentation size effect and the influence of work-hardening induced by the rolling process for riblet forming is negligible compared to the scatter of the indentation measurements.

The amount of surface residual stress, induced by the riblet rolling, was measured by X-ray diffraction using the $\sin^2(\Psi)$-method. Prior to riblet rolling, the residual stress was (-11 ± 8) MPa. Due to riblet rolling a change to (-29 ± 7) MPa was noticed.

4.2 Fatigue experiments

The results of the fatigue experiments are summarized in Fig. 3 and compared to literature values. Solid blue circles indicate results for bare Al2024 smoothened by grinding with sand paper (grit 600) prior to testing. The lifetime of these samples compares well with literature results taken from Refs [3,7] ensuring the reliability of the present measurements: Neither the adhesive connection of the samples to the testing machine, nor the thin sheet sample geometry that necessitate damping of flexural vibrations, have an influence of the sample lifetime.

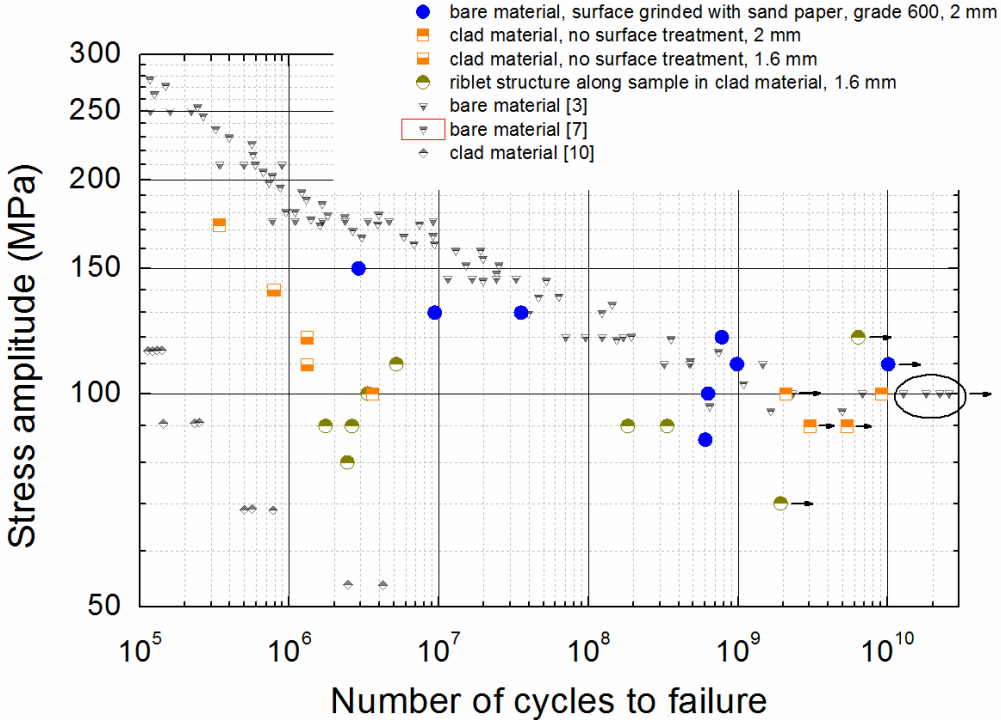

Figure 3. S/N graph of the fatigue lifetimes obtailed in the present work and from literature [3,7,10].

Just the scattering of our values seems to be slightly increased compared to the literature values.

For the clad material (orange half squares) surface smoothening is not possible without removing the cladding layer. The surface quality therefore seems to be the for lifetime reduction compared to bare Al 2024 by several orders of magnitude. Nevertheless, some samples, tested at 90 and 100 MPa, do not seem to be influenced by scratches and exhibit a much longer lifetime which lie in the same range as for the bare material. Furthermore, sample thickness in the tested range seems not to influence lifetime.

First measurements on structured samples with riblets along the sample direction (green half circles) show similar results as obtained for the unstructured clad material The fractures between 10^6 and 10^7 cycles at load amplitudes between 80 MPa and 110 MPa are is most induced by small scratches on the sample surface. Nevertheless, also run-outs above 10^8 cycles were observed in the same load regime.

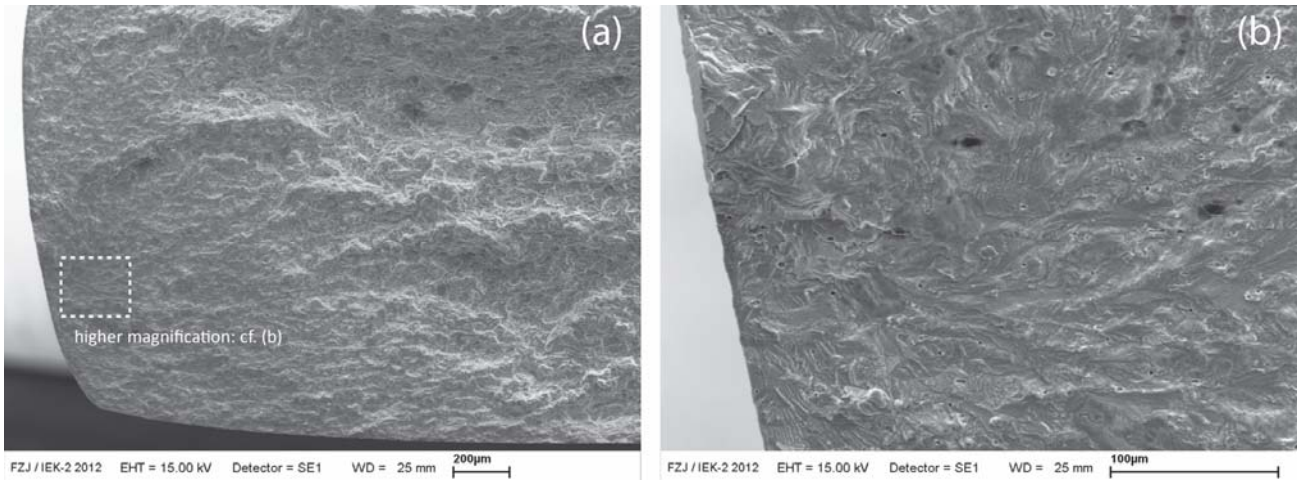

Figure 4. Fracture surface of a bare sample. $N = 9.8145 \times 10^8$, $\sigma_{max} = 110$ MPa. **(a)** Overview. **(b)** Higher magnification of the crack initiation site.

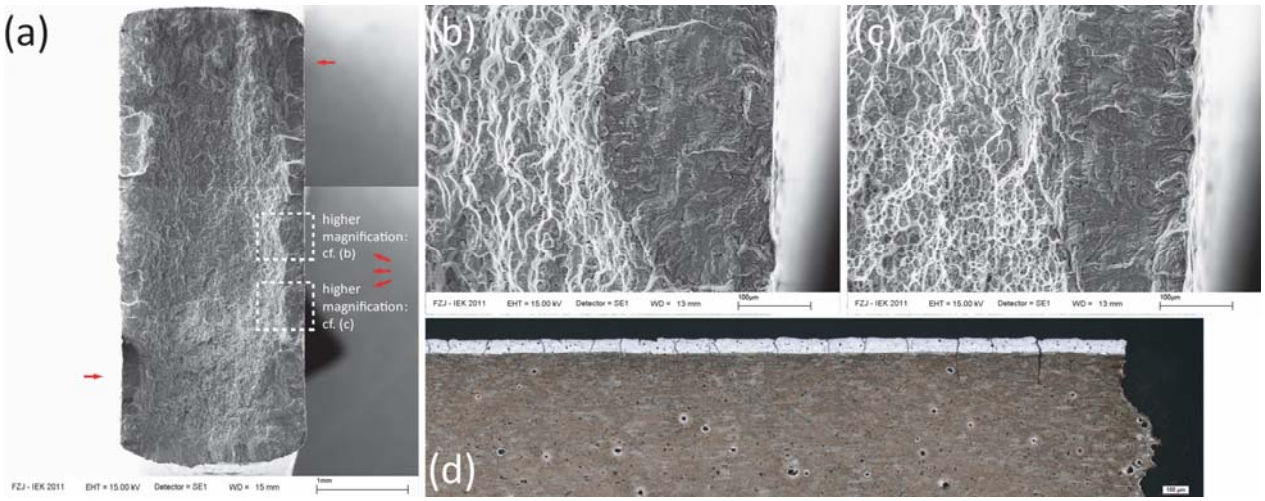

Figure 5. Fracture surface of a cladded specimen. $N = 3.38 \times 10^5$, $\sigma_{max} = 173$ MPa. **(a)** Overview Crack initiation sites are indicated by red arrows. **(b)** and **(c)** Higher magnification of crack initiation sites. **(d)** Polished longitudinal section of the same sample. The fracture plane is located on the right.

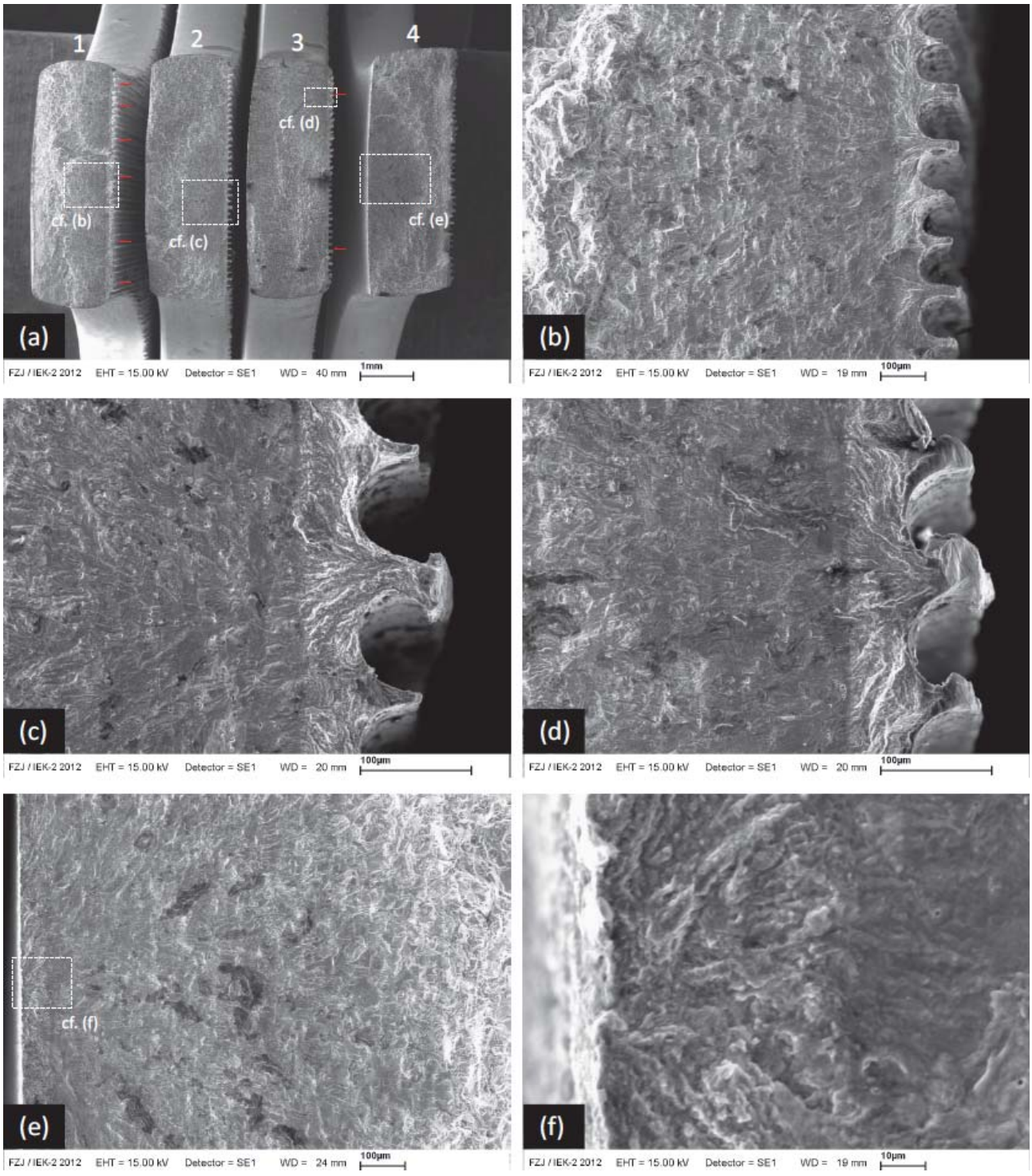

Figure 6. Fracture surfaces of structured samples. **(a)** Overview of four different specimen: (1) $N = 1.75\text{x}10^6$, $\sigma_{max} = 90$ MPa, (2) $N = 3.35\text{x}10^8$, $\sigma_{max} = 90$ MPa, (3) $N = 5.19\text{x}10^6$, $\sigma_{max} = 110$ MPa, (4) $N = 1.83\text{x}10^8$, $\sigma_{max} = 90$ MPa. Red arrows indicate crack initiation sites for samples with multiple crack initiation. **(b) – (f)** SEM images with higher magnification, showing crack initiation sites in detail.

5. Microscopy

Fig. 4 shows SEM images of a typical fatigue fracture of a bare sample at nearly 10^9 cycles. The fracture origin is located close to the surface inside the material. A magnified view of the crack initiation site is presented in Fig. 4(b). Bare samples typically show single crack initiation sites in

the VHCF-regime.
Fig. 5 shows the fracture surface of a clad sample after fatigue at relatively high load amplitude. Multiple crack initiation sites, both at the bare side and in the cladding (cf. red arrows in Fig. 5(a)) can be clearly seen. A detailed view on exemplary crack initiation sites are shown in Fig. 5(b) and (c). A polished longitudinal section of the same sample (Fig. 5(d)) illustrates multiple cracks starting at the surface of the cladding layer and crack growth into the substrate.
Failure of structured samples has been observed in two different lifetime regimes (cf. Fig. 3):(i) below 10^7 cycles and (ii) above 10^8 cycles. Fig. 6(a) gives an overview on typical fracture surfaces. Samples 1 and 3 represent the lifetime regime (i), whereas samples 2 and 4 are representative for the VHCF-regime (ii). Specimens with shorter lifetime show multiple crack initiation sites. In both cases the final fracture has its origin on the structured side close to the surface. For samples with longer lifetime, only one initiation site has been observed. In the case of sample 2 this is located on the structured side, for sample 4 on the backside, which does not have a cladding layer but a bare, smoothened surface. It is interesting to note that the lifetimes of both samples are similar to the lifetime of non-structured, bare sheets.

6. Conclusion

Fatigue experiments were performed on Al 2024 sheets with and without a pure Al cladding layer. Cold rolling of a riblet structure on the cladded side induces -if any- only slight work-hardening within the scatter of hardness measurements performed by microindentation, whereas a slight increase of compressive surface residual stress was observed after rolling. Fatigue lifetimes determined for the bare material match literature data quite well. For cladded material without riblet structure, a reduced lifetime is observed which is attributed to surface scratches which could not be removed from the thin cladding by grinding and polishing. Riblet structures produced by cold rolling do not significantly affect fatigue life of the clad material.

Bare sheets show crack initiation inside the material. Clad samples show crack initiation in the cladding layer surface and subsequent crack growth into the substrate. In general at $N < 10^7$ multiple crack initiation sites are observed, whereas in the VHCF regime only single crack initiation sites are found. Clad specimens show crack initiation both on their cladded and on their bare surface which complies well with the similar lifetimes observed for both specimen types.

Acknowledgements

The present work was funded by the Deutsche Forschungsgemeinschaft (DFG) in the framework of the DFG Research Unit 1779 “Active Drag Reduction”. The authors would like to thank H. Mayer and R. Schuller for helpful discussion on the experimental setup. Furthermore we thank T. Romans and J. Pöblau for the structuring of the sheets.

References

[1] D. W. Bechert, M. Bruse, W. Hage, J. G. T. Van Der Hoeven, and G. Hoppe, *Experiments on drag-reducing surfaces and their optimization with an adjustable geometry*, Journal of Fluid Mechanics **338**, 59 (1997).

[2] S. Klumpp, M. Meinke, and W. Schröder, *Friction Drag Variation via Spanwise Transversal Surface Waves*, Flow, Turbulence and Combustion **87**, 33 (2011).

[3] H. Mayer, M. Fitzka, and R. Schuller, *Ultrasonic fatigue testing of 2024-T351 aluminium alloy at different load ratios under constant and variable amplitude*, presented at the 5th Int. Conf. Very High Cycle Fatigue, Berlin (2011).

[4] Q. Y. Wang, T. Li, and X. G. Zeng, in *Fatigue 2010*, edited by P. Lukas (Elsevier Science Bv, Amsterdam, 2010), Vol. 2, pp. 65.

[5] T. Li, M. R. Sriraman, C. Wang, and Q. Y. Wang, *Gigacycle fatigue of precipitation hardening aluminium alloys*, presented at the Fourth international conference on very high cycle fatigue (VHCF-4), Ann Arbor, Michigan (2007).

[6] H. Mayer, *Ultrasonic torsion and tension–compression fatigue testing: Measuring principles and investigations on 2024-T351 aluminium alloy*, International Journal of Fatigue **28**, 1446 (2006).

[7] S. Stanzl-Tschegg, *Fracture mechanisms and fracture mechanics at ultrasonic frequencies*, Fatigue Fract Engng Mater Struct **22**, 1999).

[8] A. Merati, *A study of nucleation and fatigue behavior of an aerospace aluminum alloy 2024-T3*, International Journal of Fatigue **27**, 33 (2005).

[9] P. R. Edwards, M. G. Earl, and A. R. C. Britain, 1977.

[10] J. Schijve and F. A. Jacobs, *Fatigue Tests on Unnotched and Notched Specimens of 2024-T3 Alclad, 2048-T8 Alclad and 7178-T6 Extruded Material*. (Nationaal lucht- en ruimtevaartlaboratorium, 1968).

[11] G. Drossel, S. Friedrich, C. Kammer, and W. Lehnert, *Aluminium Taschenbuch: Band 2: Umformung von Aluminium-Werkstoffen, Gießen von Aluminium-Teilen, Oberflächenbehandlung von Aluminium, Recycling und Ökologie*, 15 ed. (Beuth, 2009).

[12] Alu-MATTER database, *aluminium.matter.org.uk*.

[13] M. Talia and J. E. Talia, *Crack propagation modeling for surface generated scratches in Al 2024-T3 clad alloy*, Journal of the Mechanical Behavior of Materials **8**, 117 (1997).

[14] S. E. Stanzl-Tschegg, *Ultrasonic fatigue* presented at the 6th Int. Fatigue Congress, Berlin (1996).

[15] H. Mayer, *Fatigue crack growth and threshold measurements at very high frequencies*, International Materials Reviews **44**, 1 (1999).

[16] S. Kovacs, S. Stille, D. Ernstes, and T. Beck, *Upgrading of an ultrasonic fatigue testing machine by means of early stage damage detection*, MP Materials Testing (submitted) (2012).